International Journal of Heat and Fluid Flow 31 (2010) 93–100

Contents lists available at ScienceDirect

International Journal of Heat and Fluid Flow

journal homepage: www.elsevier.com/locate/ijhff

Large Eddy simulation of a droplet laden turbulent mixing layer

W.P. Jones *, S. Lyra, A.J. Marquis

Department of Mechanical Engineering, Imperial College London, Exhibition Road, London SW7 2AZ, UK

ARTICLE INFO

Article history:
Received 19 December 2008
Received in revised form 15 July 2009
Accepted 3 October 2009
Available online 6 November 2009

Keywords:
LES
Mixing layer
Two-phase flows
Self-similarity
Preferential particle concentration

ABSTRACT

Large Eddy simulation (LES) is applied to a droplet laden turbulent mixing layer and the influence of shear, on the transport and preferential concentration of the dispersed phase is discussed. A Lagrangian formulation has been adopted for the particle dispersion coupled with an Eulerian description for the carrier gas. A stochastic model has been used to account for influence of the sub-grid scale motions of the continuous phase on the particle motion. Simulations conducted neglecting this sub-grid dispersion model show that the liquid dispersion is under predicted. However, when the sub-grid model is included the results show good agreement when compared with the experimental findings, demonstrating that the characteristics of the flow are well captured. A sensitivity analysis on the effect of the dispersion constants has been conducted, suggesting that increasing the contribution of the stochastic term, leads to a higher accumulation of smaller particles at the edge of the mixing layer.

1. Introduction

Two-phase flows are encountered in many practical systems with industrial, environmental and biomedical applications. Examples of such flows include the dispersion of pollutants in the atmosphere, the transport of liquid spray droplets in internal combustion engines and jet engine combustors, the dilution of medicines by blood through the vessels and dust inhalation into human lungs. Industrial and aircraft gas turbines in particular, are fuelled by liquid hydrocarbons making spray atomisation and evaporation crucial phenomena in the analysis of combustion dynamics.

Over the past decades, extensive experimental and theoretical studies have been performed to determine the response of particles (solid or liquid) in shear flows and the modification of turbulent characteristics, in a number of different geometrical configurations such as turbulent jets, boundary layers and mixing layers, Chung and Troutt (1988), Kulick et al. (1994). Mixing layers in particular, are characterised by the presence of large-scale stream and spanwise vortical structures, with size comparable to the transverse length scale of the flow, that play a dominant role in the particulate dispersion process and whose interaction causes the growth of the mixing region, Brown and Roshko (1974). The effects of these structures on solid particle dispersion has been studied by Chein and Chung (1987), Lazaro and Lasheras (1992) concluding that the dispersion phenomena are strongly dependent on the size of the particulate phase. Squires and Eaton (1991a) investigated the preferential concentration of solid particles in high strain regions, in terms of the Stokes number while Kiger and Lasheras (1997) examined the additional dissipation of the kinetic energy occurring due to interphase energy transfer in dilute particle laden shear flows. Despite the numerous experimental efforts, several aspects governing the interaction of liquid droplets or solid particles on a carrier gas phase remain unsolved as it is often difficult to isolate the momentum exchange between particles and gas from the production and dissipation mechanisms in a turbulent flow.

Consequently, numerical simulations for the prediction of the interactions between particles and turbulence and the modulation of turbulence due to the particles' motion have received increasing attention. Direct numerical simulation (DNS) of particle transport in homogeneous isotropic stationary, Squires and Eaton (1990, 1994), or decaying, Elghobashi and Truesdell (1993), turbulence with two-way coupling between the gaseous and the discrete phase suggests that the presence of particles increases the turbulent kinetic energy at high wave numbers and decreases it at low wave numbers and that the distortion of the turbulence energy spectrum depends on parameters such as the particle relaxation time. Later studies, Squires and Eaton (1991b), focused on the particle dispersion, turbulence modulation and preferential concentration of solid particles or liquid droplets and demonstrated that the mixing of particles by turbulence depends strongly on the relative timescales of the two phases.

Despite the fact that DNS studies can provide a detailed description of two-phase flows, they are still very expensive computationally, even when a moderate number of particles is considered. Large Eddy simulation (LES) is a promising tool for the prediction

* Corresponding author. Tel.: +44 0207594 7037.
E-mail address: w.jones@imperial.ac.uk (W.P. Jones).

0142-727X/$ - see front matter © 2009 Elsevier Inc. All rights reserved.
doi:10.1016/j.ijheatfluidflow.2009.10.001

of turbulent flows as it is less computationally demanding and has proved able to provide an accurate description of turbulent mixing. In LES, direct simulation techniques are applied to determine precisely the contribution of the large-scale flow features, which are assumed to be the most important with respect to momentum and energy transport in turbulent flows. A spatial filter is applied to the governing equations, in order to eliminate the need to solve the contribution of the scales smaller than the filter width, Piomelli (1999). The LES equations that describe two-phase flows include terms that represent the sub-grid fluctuations of the continuous phase and the filtered source terms arising from the contribution of the dispersed phase. Several LES studies, Wang and Squires (1996), Uijttewaal and Oliemans (1996), Wang and Squires (1998), Yeh and Lei (1991a,b), have been conducted taking into account only the effects of the resolved scales and neglecting the influence of the unresolved scales on the particle motion, under the assumption that the trajectories of the heavy particles ($St \gg 1$) are not affected by the smaller turbulent scales due to their inertia, despite the fact that in these simulations small particles ($St \sim 1$), were also considered. Fundamental studies, Miller and Bellan (2000), have shown that the sub-grid effects on the droplet transport in turbulent shear flows cannot be neglected as significant errors are introduced in the prediction of the droplet drag force and evaporation rates if they are omitted. As a consequence for small droplets the interactions between turbulence, spray dispersion, vapour micro-mixing and combustion that occur at scales much smaller than the filter width can be significant and models are thus required for sub-grid scale effects on droplet break-up, dispersion and evaporation.

The present study aims to investigate numerically, by the use of LES, a spatially evolving, turbulent, droplet laden mixing layer and focuses on the influence of shear, on the transport and preferential concentration of the dispersed phase. The liquid phase is tracked in a Lagrangian reference frame, whereas the gas phase flow variables are solved in an Eulerian reference frame. A stochastic model has been used for the representation of the effects of the unresolved scales on the droplet motion.

The model involves a Weiner process in which the diffusion coefficient is a function of the sub-grid turbulence kinetic energy and a particle 'Eddy-interaction' timescale. This timescale is dependent on the sub-grid timescale and the particle relaxation time and involves two constants, C_o which is of the order of unity and α which has been assigned a value 0.8. Previous studies, Bini and Jones (2008), have discussed the effect of the stochastic term on the normalised liquid concentration in similar shear flows, concluding that if it is neglected the particle diffusion is underestimated. In addition, the influence of the 'Eddy- interaction' timescale has been investigated, where it was demonstrated to have a significant effect on the particle acceleration probability density function, *pdf*. Moreover, Bini and Jones (2007), suggested that for particles transported in isotropic turbulence a value of $\alpha = 0.8$ reproduces accurately the heavy tailed *pdfs* observed experimentally. The present work builds upon previous findings and aims to investigate the effect of the sub-grid dispersion model on the quantities that characterise a turbulent droplet laden mixing layer and in particular, focuses on the sensitivity of the results to the values of the constants, α and C_o. The dispersed phase is composed of discrete spherical droplets, has a relatively small volume fraction and as a consequence droplet collisions, breakup and coalescence effects are negligible.

The structure of this paper is as follows. The mathematical formulation and the assumptions involved in the modelling of the particle dispersion in a turbulent gas carrier phase as well as the *pdf* approach for the dispersed phase are presented in the next section. The experimental apparatus used in the test case examined, the computational details of the simulations, the predictions of the calculations and the comparison with the experimental data are presented and discussed in the third section. The conclusions of the study are summarised in the final section.

2. Modelling

2.1. Filtered Navier–Stokes equations

In LES, a spatial filter is applied to the Navier–Stokes equations. The filtering operation is defined as

$$\bar{f}(\mathbf{x},t) = \int_{\Omega} G(\mathbf{x}-\mathbf{x}';\Delta(\mathbf{x}))f(\mathbf{x}',t)d\mathbf{x}', \tag{1}$$

where G is the filter function and Δ is the filter width assigned as the cube root of the local cell volume, Germano et al. (1991). In flows where large density fluctuations occur, the introduction of density filter quantities is essential and are defined as: $\tilde{f} = \overline{\rho f}/\bar{\rho}$.

The density weighted filtered Navier–Stokes equations with the contribution of the dispersed phase, as point sources of mass momentum and energy can be written as:

$$\frac{\partial \bar{\rho}}{\partial t} + \frac{\partial(\bar{\rho}\tilde{u}_i)}{\partial x_i} = \bar{S}_{mass}. \tag{2}$$

$$\frac{\partial(\bar{\rho}\tilde{u}_i)}{\partial t} + \frac{\partial(\bar{\rho}\tilde{u}_i\tilde{u}_j)}{\partial x_j} = -\frac{\partial \bar{p}}{\partial x_i} + \frac{\partial \bar{\sigma}_{ij}}{\partial x_j} + \tilde{\tau}_{ij} + \bar{\rho}g_i + \bar{S}_{mom,i}. \tag{3}$$

The Smagorinsky (1963) model is used for the sub-grid scale tensor: $\tau^d_{ij} = -2\mu_{sgs}\widetilde{S}_{ij}$, where τ^d_{ij} is the deviatoric *sgs* stress with $\mu_{sgs} = \bar{\rho}(C_s\Delta^2)\|\widetilde{S}_{ij}\|$. C_s is the Smagorinsky constant equal to 0.07 and $\|\widetilde{S}_{ij}\|$ is the Frobenius norm $\|\widetilde{S}_{ij}\| = \sqrt{2\widetilde{S}_{ij}\widetilde{S}_{ij}}$ of the filtered strain tensor, $\widetilde{S}_{ij} = 0.5\left(\frac{\partial \widetilde{U}_i}{\partial x_j} + \frac{\partial \widetilde{U}_j}{\partial x_i}\right)$. Dynamic versions of the Smagorinsky model, Germano (1992), Piomelli and Liu (1995), allow the value of the parameter C_s to be determined as a function of time and position. However, there is little to be gained by the use of more complex *sgs* models in the case of high Reynolds number free flows of the type considered. As is clear from the results presented below the standard Smagorinsky model gives good results for mixing layer flows.

The source terms appearing in the gas phase equations can be evaluated as: $\bar{S} = \frac{1}{\Delta^3}\sum_{i=1}^{n} S^{(\alpha)}$, where the summation is over the number of the droplets present in the cell volume under consideration and S^{α} is the source term arising from the α-th droplet which can be written as:

$$S^{\alpha}_{mass} = -\frac{dm^{(\alpha)}}{dt}, \tag{4}$$

$$S^{\alpha}_{mom,i} = -\frac{d}{dt}(mu_i)^{(\alpha)}. \tag{5}$$

The source term in the momentum equation accounts for two-way coupling between the gas and liquid phase. In dilute flows, such as that presently considered, the effects of this coupling are negligible and the term could almost certainly be omitted without loss. It is however, retained for completeness.

2.2. PDF modelling of fuel sprays

Following Bini and Jones (2008) the dispersed phase is described through a set of independent macroscopic variables, the droplet radius r, the droplet number n, the droplet velocity $\mathbf{v}$ and the droplet temperature θ. The Weber number is presumed small enough, $We < 20$, so the droplets have a spherical shape. The evolution of the filtered joint *pdf* $\bar{P}(R,N,\mathbf{V};\mathbf{x},t)$ is derived using the fine-grained probability density function approach, Lundgren (1967), *i.e.*:

$$\frac{\partial \overline{P}}{\partial t}+\frac{\partial}{\partial \mathbf{V}_j}(a_j\overline{P})+\frac{\partial}{\partial N}(\dot{N}\overline{P})+\frac{\partial}{\partial R}(\dot{R}\overline{P})+\frac{\partial}{\partial \Theta}(\dot{\Theta}\overline{P})=0, \tag{6}$$

where a_j is the particle acceleration, $\dot{N}=dn/dt$ is the rate of change of the droplet number through the process of droplet breakup and coalescence, $\dot{R}=dr/dt$ the rate of change of the droplet size through evaporation and $\dot{\Theta}=d\theta/dt$ the rate of change of droplet temperature caused by heat transfer from the surrounding gas phase. Eq. (6) is an exact 'unclosed' hyperbolic partial differential equation for the joint *pdf* of the spray, unclosed because the filtered conditional Lagrangian rates of change are unknown.

In the cases considered the droplets are significantly smaller than the filter width and the LES of the carrier phase only provides the filtered flow-field at the particle position. Since the interactions between the carrier and discrete phase, occur at a scale much smaller than the filter width, the sub-grid scale, *sgs*, fluctuations in velocity and scalar quantities such as temperature and mixture composition of the carrier flow field dominate and their influences on the droplet dynamics must be modelled. However, in isothermal dilute cases, such as that considered here, evaporation, break-up or coalescence phenomena are negligible and models for $\dot{N},\dot{R}$ and $\dot{\Theta}$ are then not required. As in Bini and Jones (2008) the conditional particle acceleration a_j is modelled as the sum of a deterministic term, evaluated in terms of filtered flow field quantities, and a stochastic contribution, with the latter representing the (non-linear) influence of the sub-filter scale velocity fluctuations.

In order to solve the modelled form of the resulting Fokker–Planck Eq. (6) it is first replaced by an equivalent system, Gardiner (2002) of ordinary differential equations describing the evolution of stochastic particles. The *Itô* equivalent of the closed form of Eq. (6) that describes the evolution of the spray *pdf* in space and time is given by the following system of equations:

$$\begin{aligned} d\mathbf{x}^{(p)} &= \mathbf{v}^{(p)}dt,\\ d\mathbf{v}^{(p)} &= \mathbf{a}^{(p)}dt, \end{aligned} \tag{7}$$

where p represents the pth particle. Consistent with this the motion of a stochastic particle in a turbulent flow field can be viewed as a random process with position determined by a deterministic part, evaluated in terms of filtered values and a stochastic component arising from the *sgs* turbulent motions of the gas phase. In this study only viscous drag and gravitational forces are considered and a stochastic Markov model is used to represent the influence of the unresolved carrier gas velocity fluctuations experienced by a stochastic particle p over a time dt, Bini and Jones (2007, 2008), which is added to the deterministic contribution:

$$d\mathbf{v}^{(p)}=\tau_p^{-1}(\widetilde{\mathbf{U}}_p(t)-\mathbf{v}^{(p)})dt+\mathbf{g}dt+\left(C_o\frac{k_{sgs}}{\tau_t}\right)^{1/2}d\mathbf{W}_t, \tag{8}$$

where $\mathbf{v}^{(p)}$ is the velocity of the p^{th} particle, $\widetilde{\mathbf{U}}_p$ is the filtered gas velocity at the particle position, k_{sgs} is the unresolved kinetic energy of the gas phase, C_o is a model constant, $d\mathbf{W}_t$ represents the increment of the Wiener process, $\mathbf{g}$ is the gravitational acceleration and τ_t is a sub-grid timescale which determines the rate of interaction between the particle and turbulence dynamics, defined as:

$$\tau_t=\tau_p\left(\frac{\tau_p}{\frac{\Delta}{\sqrt{k_{sgs}}}}\right)^{2\alpha-1}. \tag{9}$$

The particle relaxation time, τ_p is given by: $\tau_p^{-1}=\frac{3}{8}\frac{\rho_f C_D}{\rho_p R}|\widetilde{\mathbf{U}}_p-\mathbf{v}^{(p)}|$, where the drag coefficient C_D is obtained from Yuen and Chen (1976):

$$C_D=\begin{cases}\frac{24}{Re}\left(1+\frac{Re^{2/3}}{6}\right): & 0<Re<1000,\\ 0.44: & Re\geqslant 1000,\end{cases} \tag{10}$$

where Re is the Reynolds number based on the droplet diameter and the relative velocity of the droplet with respect to the gas phase.

The *sgs* kinetic energy is obtained from $k_{sgs}=(2\Delta v_{sgs}\widetilde{S}_{ij}\widetilde{S}_{ij})^{\frac{2}{3}}$, an expression derived using equilibrium arguments.

Eq. (8) provides a modelled and complete description of the droplet motion in a turbulent flow field, accounting for viscous and gravitational forces. Once the droplet dynamics have been defined and the instantaneous relative droplet-gas velocity has been calculated, it is possible to calculate the rate of change of the droplet temperature and diameters as well as the rate of change of the number of droplets per liquid unit mass that may occur through collisions and droplet break-up. However, in the presently considered dilute, isothermal flows such phenomena are neglected.

3. Results and discussion

The case considered in the present work corresponds to a planar mixing layer, studied experimentally by Tageldin and Cetegen (1997), formed between two ambient temperature air streams with a velocity ratio of 0.28. The experimental configuration and the measurement zone are presented in Fig. 1. The test section consists of a vertically oriented 200 mm long square duct with a 150×150 mm cross section. Honeycomb flow straighteners and a set of fine mesh screens were placed upstream of the splitter plate trailing edge. The fastest air stream was seeded with water droplets with a Sauter Mean Diameter of 35 μm, by means of an array of 12 miniature atomisers located upstream of the measurement zone. The operating temperature was selected to prevent evaporation. The resulting spray flow is characterised as dilute, with a volumetric void fraction of 5.5×10^{-6} therefore droplet collisions and coalescence phenomena are negligible.

The LES in-house code BOFFIN, Jones et al. (2002), was used for the computations conducted. The computational domain, consisted of $150\times80\times60$ nodes in the x,y,z directions, respectively and corresponds to the region $0<x<200$ mm, $-75<y<75$ mm and $0<z<150$ mm of the physical domain, where the measurements were conducted. The grid was uniformly spaced in the z-direction and stretched in the x- and y-directions, allowing for a finer spacing close to the injection place and in the region around

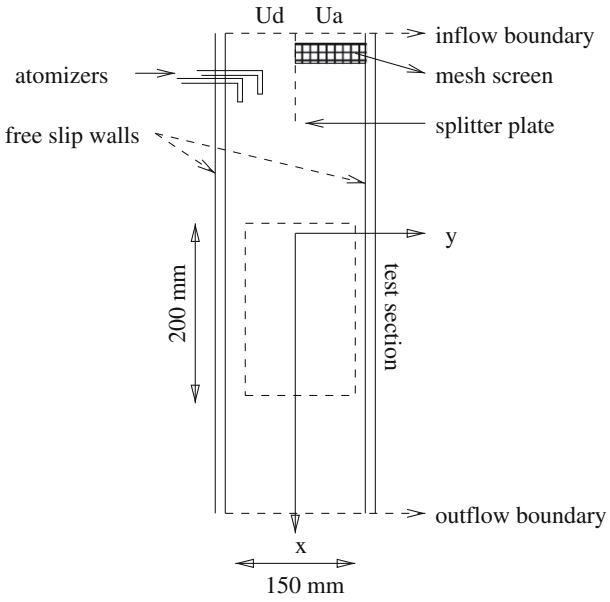

Fig. 1. Experimental configuration.

$y = 0$ mm, where the mixing takes place. The grid expansion rates were chosen to be close to unity so as to avoid commutation errors. In the present simulation, the Reynolds number based on the momentum thickness is 225 and the filter width varies between $\Delta = 0.9$ mm in the regions closer to the shear layer, where higher resolution is required, to $\Delta = 1.3$ mm in regions away from the mixing region. This can be compared with the filter widths used in previous related studies. For example single phase LES studies of the temporal mixing layer have considered filter widths as large as $\Delta = 1.4$ mm, Jimenez et al. (1997) and $\Delta = 1.1$ mm, Vreman et al. (1997), whereas two-phase DNS studies, Miller and Bellan (2000), used widths varying from $\Delta = 0.66$ mm to $\Delta = 1.9$ mm for Reynolds numbers based on the initial momentum thickness in the range of 200–600.

At the inflow plane $x = 0$, the flow is fully developed with turbulence intensity of 2% based on the mean velocity in the droplet seeded stream, and 4–5% in the unseeded gas stream. In order to apply realistic turbulent inflow conditions an inflow generator, based on digital filters was used, di Mare et al. (2006). The method generates spatially and temporally correlated turbulent structures, used as instantaneous inflow velocity profiles that reproduce, when averaged, the specified mean and Reynolds stress profiles. At the outflow boundary, $x = 200$ mm, convective outflow conditions were applied, $\frac{\partial u_i}{\partial t} + U_c \frac{\partial u_i}{\partial n} = 0$, where n is the direction normal to the boundary and U_c is the mean convective velocity calculated from the mass conservation equation.

The governing equations for the carrier gas are solved numerically using second order accurate central difference schemes to represent the spatial derivatives. The transient term is discretised according to a three-point backward scheme. The code employs Cartesian velocity components with co-located variable storage arrangement and it is based on a fully implicit low Mach number formulation. For the particle transport equation an Euler scheme is used, consistent with *Itô* calculus. The Weiner process, ΔW_t is represented by $\eta \times \sqrt{\Delta t}$, where η is a random vector sampled from a normalised Gaussian distribution independent for each time step. The dispersed phase is represented by a large number of stochastic particles. During each time step, the continuous phase fields are first updated and then are interpolated to the particle position using a trilinear interpolation scheme and passed to the Lagrangian solver. The time averaged statistical properties of the liquid phase are obtained by first locating the particles and then by computing ensemble averages from the set of particles present in each finite volume cell. Time averaging over several flow through times is carried out in order to determine the statistics needed for comparison purposes. After the start-up of the simulation as many as 4×10^6 droplets were present in the domain during each flow through time.

At every time step droplets are injected at the inlet plane at a rate consistent with the required liquid volumetric flow rate. The droplet diameter *pdf*, measured at discrete y positions is well represented by the Nukiyama–Tanasawa distribution function, Lefebvre (1989).

$$p(D) = aD^p e^{-(bD)^g}, \tag{11}$$

by suitable selection of the parameters p, b, g, see Fig. 2.

Turbulent mixing layers are known to be self-similar, characterised by suitably normalised turbulent statistics that are independent of the downstream position and a linear growth of the layer thickness. The downstream spreading can be defined in terms of two quantities: the layer thickness and the momentum thickness in terms of the mean droplet velocity profiles, calculated as:

$$\delta_{08}(y) = y\left(\frac{U_d}{U_{d\infty}} = 0.1\right) - y\left(\frac{U_d}{U_{d\infty}} = 0.9\right), \tag{12}$$

$$\theta_u(y) = \int_{-\infty}^{\infty} \frac{U_d}{U_{d\infty}}\left(1 - \frac{U_d}{U_{d\infty}}\right) dy. \tag{13}$$

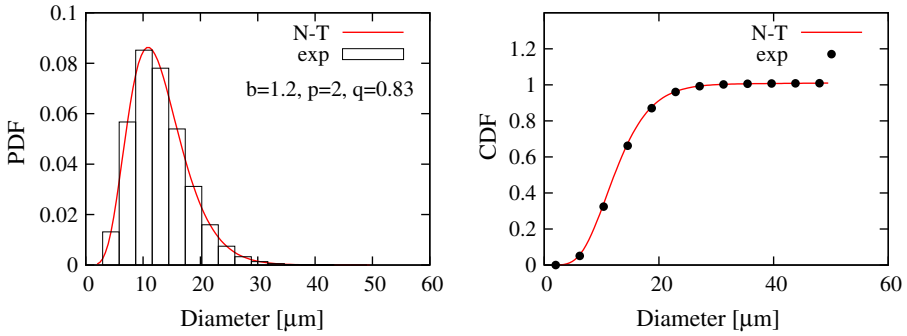

Fig. 2. Droplet size distribution.

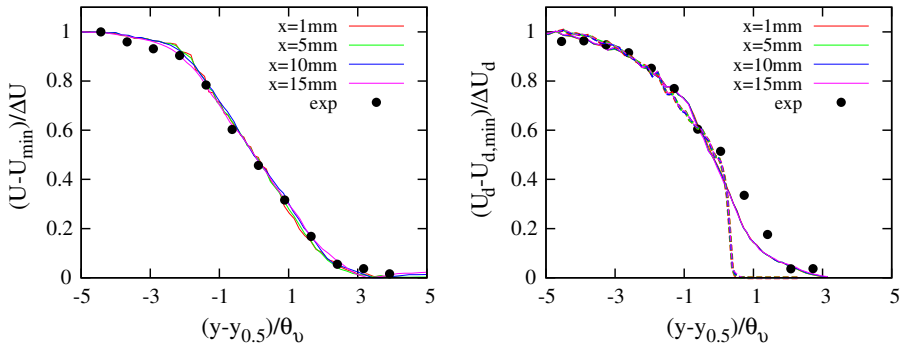

Fig. 3. Normalised stream wise velocity profiles for the gas (left) and the dispersed (right) phase: experimental data (symbols) and computed results (lines). The dashed lines refer to the case in which the sub-grid dispersion model is omitted.

Fig. 3, where U_{min} is the minimum value of the velocity U and $y_{0.5}$ is the location at which $U = \Delta U/2$ and where the index d corresponds to the dispersed phase, shows computed and experimental mean (time averaged) gas and droplet velocity cross stream profiles at selected downstream stations, located in the near-field of the mixing layer. This is the important region in many combustion processes related particularly to ignition and flame stabilisation, Lopéz-Pagés et al. (2004). Following the experimental procedure of Tageldin and Cetegen (1997), the profiles are presented in similarity coordinates, scaled with the momentum thickness θ_u and the velocity difference ΔU across the layer, respectively. The results shown are obtained with the sub-grid dispersion model constants $C_o = 1.0$ and $\alpha = 0.5$. Simulations were also conducted with sub-grid dispersion neglected completely and the resulting profiles are presented at the four downstream, locations, indicated by the dashed lines in Fig. 3. The profiles evolve in a self-similar manner as expected but in this case, the dispersion at the shear layer is significantly underestimated. In contrast when the sub-grid dispersion model is incorporated the predicted profiles are in good agreement with the experimental findings and independent of the downstream distance, preserving the self-similarity of the flow and reproducing the liquid droplet dispersion as measured experimentally.

Predicted and measured profiles of the layer thickness, δ_{08} and momentum thickness, θ_u are presented in Fig. 4a and b, respectively and for the 'centreline' position, $y_{0.5}$ in Fig. 5. All three quantities are observed to increase linearly with downstream distance and the layer thickness δ_{08} and the 'centreline' penetration $y_{0.5}$ are found to be greater in magnitude by a factor of five compared to the momentum thickness. At the origin of the layer, the 'centreline' is shifted towards the fast stream due to the initial boundary layer effects consistent the experimental results. Results are shown for cases with the sub-grid dispersion model both included and omitted ($C_o = 0$). The influence of the parameter C_o was investigated and results are presented for $C_o = 0.5, C_o = 1$ and $C_o = 2$. The linear growth of the layer is reproduced by all calculations and when the sub-grid dispersion model is included the results of the simulations are in excellent agreement with measurements regardless of the value of C_o; the effects of varying C_o in the range $0.5 < C_o < 2$ on the spreading rate are found to be negligible. On the other hand when the sub-grid dispersion model is omitted large discrepancies between simulation and experiment are evident; the spreading of the liquid phase is significantly under predicted.

An important parameter in the dispersion of particles by turbulence is the particle size. The ratio of drag to inertial forces acting on a small particle is inversely proportional to the square of its diameter. Therefore, very small particles, behave like a passive scalar. Large particles, due to their high inertia will hardly be dispersed. Particles with diameter between these two limits, will be partially affected by the turbulence. The probability density function of the particle population gives information about the concentration of the different particle sizes along the mixing region. Following the experimental results, the evolution of this function at two cross-stream locations plotted for several downstream locations is given in Figs. 6 and 7. At each downstream location, the dispersion region close to the undisturbed spray has a *pdf* with a higher percentage of small particles, suggesting that the dispersion is a size-selective process.

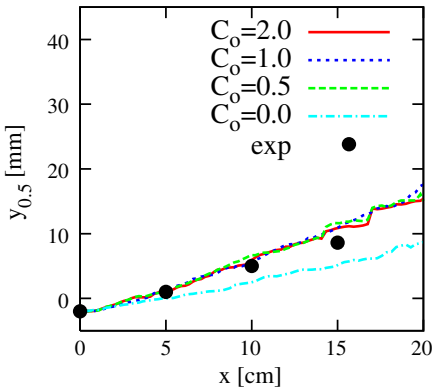

Fig. 5. Dependence of the longitudinal evolution of the centreline penetration on the dispersion constant C_o: experimental data (symbols) and computed results (lines).

Fig. 6 compares measured and predicted droplet size distributions, in the fast stream of the mixing layer ($y < 0$ mm) at the shear layer ($y = 0$ mm) and in the slow stream ($y > 0$ mm) at three selected downstream locations $x = 1$ cm, $x = 5$ cm and $x = 15$ cm. A parametric investigation was conducted on the influence of the constants C_o, and a on the particle diffusion (Eq. 8). Results are presented with and without the sub-grid dispersion model. The results of five different computations are presented, corresponding to cases, where (a) $C_o = 1$ and $\alpha = 0.5$, (b) $C_o = 1$ and $\alpha = 0.8$, (c) $C_o = 2$ and $\alpha = 0.8$, (d) $C_o = 0.5$ and $\alpha = 0.8$ and (e) $C_o = 0$ and $\alpha = 0.5$. The simulations with the sub-grid dispersion term included, cases (a–d), result in predictions in very good agreement with the experimental data in the the fast and slow stream regions ($y < 0.0$ mm) and ($y > 0.0$ mm) with the predictions of the selective dispersion of different droplet size classes being accurately reproduced. Sensitivity analysis showed that the effect of changes in the parameter α, with the value of C_o held constant, causes a change of less than 2% in the particle concentration distribution. The maximum deviation, compared to the experimental data, of the particle distribution at locations in the fast and slow regions

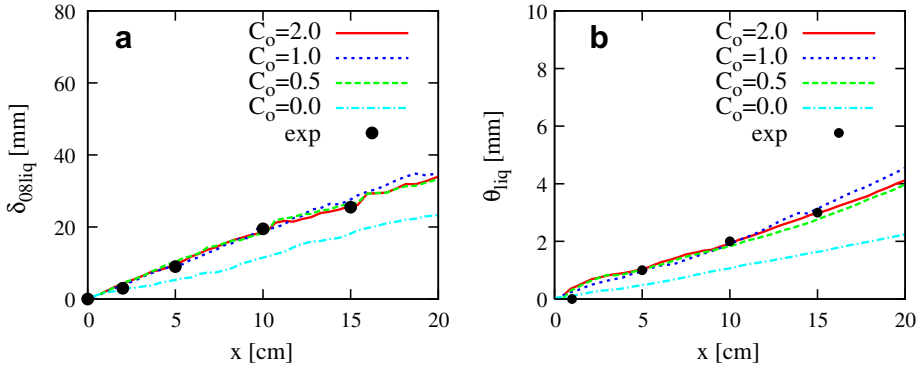

Fig. 4. Dependence of the longitudinal evolution of the (a) velocity thickness and (b) momentum thickness on the dispersion constant C_o: experimental data (symbols) and computed results (lines).

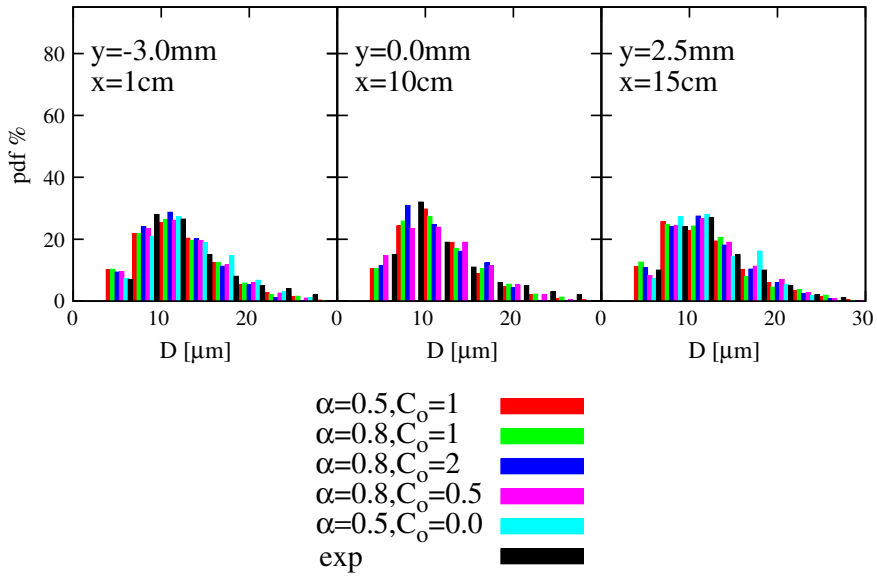

Fig. 6. Probability density function of the droplet diameters at downstream locations $x = 1.0$ cm, $x = 10.0$ cm and $x = 15.0$ cm in the fast stream zone (left), at the edge of the layer (middle) and in the slow region (right).

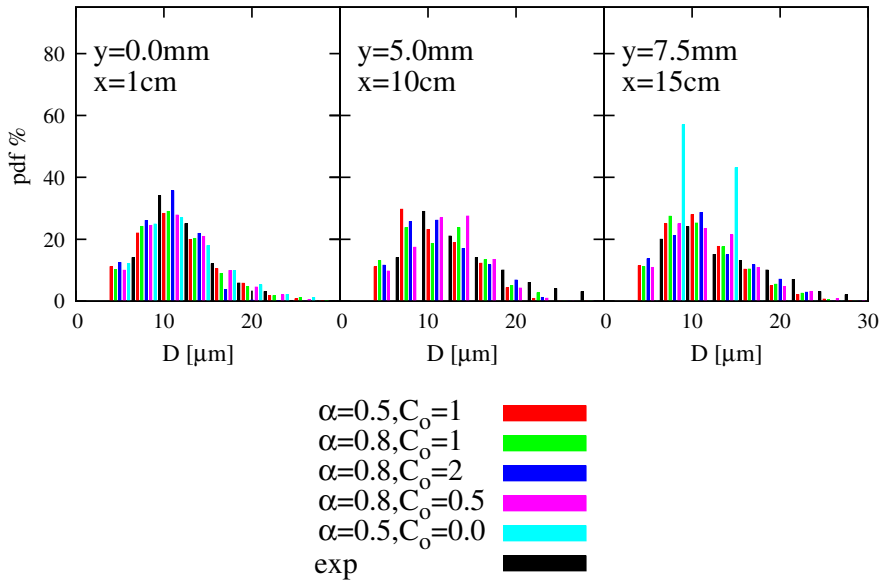

Fig. 7. Probability density function of the droplet diameters at downstream locations $x = 1.0$ cm, $x = 10.0$ cm and $x = 15.0$ cm at the edge of the layer (left), in the fast stream zone $y = 5.0$ mm (middle) and $y = 7.5$ mm (right).

for the different values of C_o, was found to be 2% and 3%, respectively. Thus the results were found not to be strongly dependant on the selection of the dispersion constants, though the inclusion of the sub-grid dispersion model is essential if accurate results are to be obtained. In contrast in the case (e), where the sub-grid dispersion model is not used, since the dispersion of the droplets is under predicted, there were locations, where the calculation of the *pdf*'s was impossible. In detail, for locations close to the injection plane ($x = 0$ mm) both in the fast stream region, ($y < 0$), and at the edge of the shear layer ($y = 0$) the predicted droplet distributions are found to be in good agreement with the measurements. At the measurement location further downstream at $x = 10$ cm no droplets were detected either at the edge of the layer ($y = 0$) and in the slow stream region and the *pdf* cannot be constructed. On the other hand, at the measurement locations close to the exit of the domain $x = 15$ cm, a large vortex was found to be formed, forcing particles to be transported towards the slow stream region ($y > 0$). At this downstream location and at ($y = 2.5$ mm), the *pdf* is found to be well reproduced in contrast to the situation inside the slower moving stream region at ($y = 7.5$ mm), where only two droplet classes are found to accumulate.

At the edge of the mixing layer an increase of the dispersion constant C_o, from 1.0 to 2.0, (with $\alpha = 0.8$), is found to shift the distribution towards smaller particle sizes suggesting that the contribution of the sub-grid dispersion model becomes more dominant for smaller particles. The effect of the dispersion coefficient on the size selective dispersion is coupled with the effect of the particle response time τ which is inversely proportional to the droplet radius R. As expected, a smaller value of the constant ($C_o = 0.5$) increases the proportion of larger particles that accumulate in the shear layer.

A high concentration of small droplets ($d \leqslant 10$ μm) is observed at $x = 1.0$ cm (62%) ($y = 0.0$), which increases by 6% as the flow moves downstream $x = 10.0$ cm. This effect, was also observed in

the experiment and it is attributed to the rapid dispersion of the small size droplets into the early part of the mixing layer since small droplets due to their smaller inertia respond faster to the turbulent fluctuations and travel further in the slow air stream.

Fig. 7 compares measured and predicted droplet size distributions, at the shear layer ($y = 0$) and in the low speed stream ($y > 0$) at $x = 1$ cm, $x = 5$ cm and $x = 15$ cm. At $x = 1$ cm and at $y = 0$, 73% of the droplets' population has $d \leqslant 10$ μm. At measurement locations further downstream and towards the slow moving air stream the presence of small droplets is still dominant but the accumulation level is found to be reduced by 9% and 14%, respectively.

Fig. 8 shows the evolution of the probability density function at $x = 150$ mm and at selective intervals across the cross-stream direction y. It can be seen that as the calculation interval is changed moving from the fast stream region towards the edge of the layer and the slow stream region, the accumulation of small particles increases by 5%.

The size-selective dispersion phenomena can be further investigated in terms of the Stokes number. For each droplet class the respective Stokes number, in terms of density of the dispersed phase ρ_d, the gas viscosity μ, the velocity difference across the layer ΔU and the mixing layer thickness δ_{08}, $St = \frac{\rho_d d^2 \Delta U}{18\ \mu \delta_{08}}$ was computed and compared with the experimental data in Fig. 9. In a turbulent flow, droplet motion is directly connected to the ability of the droplet to respond to the large turbulent structures of the flow, Longmire and Eaton (1992). Small Stokes numbers (e.g. $\ll 1$) indicate that the particle motion is dominated by the fluid flow via the drag and lift force acting on the particle, therefore the particle follows the fluid motion with little slip velocity and droplets behave essentially as fluid elements. A large Stokes number indicates that the particle inertia is dominant and that the fluid motion does not exert a significant affect the particle behaviour, Elghobashi (1994), Martin and Meiburg (1994).

Stokes numbers are found to agree well with the experimental findings and to increase with increasing droplet size at a given location x. Droplets in the size class 2–10 μm exhibit a Stokes number ranging from 0.08 at the exit of the domain to 1.2 in the near-field of the mixing layer, findings which are consistent with the higher accumulation of small droplets at the slow stream zone of the layer close in the early part of the mixing layer. The decrease in the Stokes number, rapidly in the beginning and then gradually, with increasing downstream distance, is due to the continuous increase of the level thickness δ_{08} that characterises the spreading of the mixing layer.

The evolution of the non-dimensional liquid volume flux with the downstream distance is presented in Fig. 10, where q_{min} is the minimum value of the volume flux q, $y_{0.5}$ is the location of the mixing layer at which $U = \Delta U/2$ and θ_{lq} is the integral volume flux thickness. Results are presented with and without the sub-grid dispersion model. In both simulations the profiles evolve in a self-similar manner but the neglect of the sub-grid contribution leads to a steeper profile and insufficient droplet 'diffusion' compared to the measured profiles. The dispersion of the liquid phase along the stream-wise direction, presented in terms of the integral volume flux thickness is depicted in Fig. 11. After an initial transient stage, the volume flux thickness of the mixing layer grows linearly with distance and is mainly dominated by large scale vortex struc-

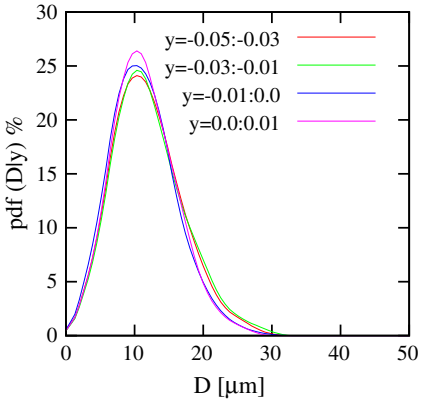

Fig. 8. Probability density function of the droplet diameters at $x = 15.0$ cm and at different y intervals.

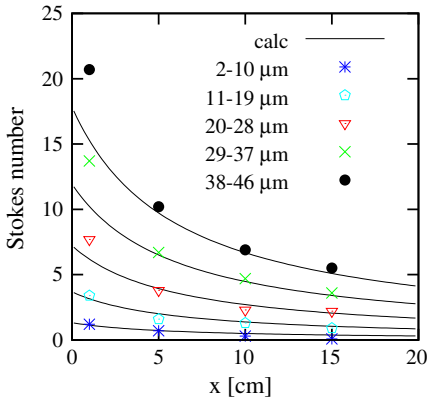

Fig. 9. Calculated and experimental longitudinal evolution of the Stokes number with downstream location as a function of the droplets' diameter.

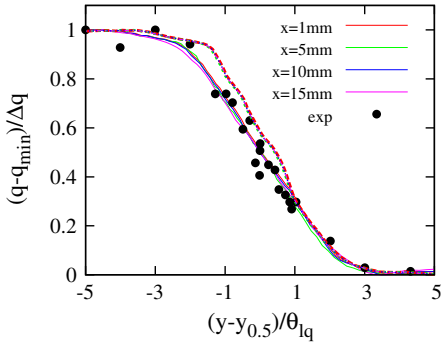

Fig. 10. Normalised liquid volume flux profiles: experimental data (symbols) and computed results (lines). The dashed lines refer to the case in which the sub-grid dispersion model is omitted.

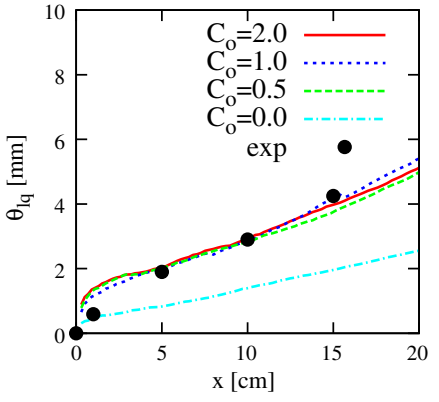

Fig. 11. Dependence of the longitudinal evolution of the integral volume flux thickness on the dispersion constant C_o: experimental data (symbols) and computed results (lines).

tures resulting in the linear growth of the layer thickness with the downstream distance. The effect of varying the value of the parameter C_o was investigated and the results suggests that the model is relatively insensitive to the values in the range $0.5 < C_o < 2.0$. However, it is evident that the integral volume flux thickness is significantly underestimated when the sub-grid dispersion term is not included.

4. Conclusions

A detailed numerical investigation of the spreading behaviour of liquid droplets, in a vertically orientated mixing layer using large Eddy simulation was conducted. It was found that the droplet dispersion is highly dependent on the sub-grid turbulent scales which cannot be neglected if good agreement with measurements is to be achieved. A stochastic sub-grid dispersion model was incorporated to simulate the effects of the filtered, unresolved scales on the particle dispersion and two-way coupling was implemented for the interaction between the carrier and discrete phase. It is shown that the LES model proposed by Jones and Sheen (1999), Bini and Jones (2007, 2008) accurately reproduces droplet dispersion and represents the size-selective phenomena occurring in shear flows. The calculations are in good agreement with the experimental findings of Tageldin and Cetegen (1997). The model was found to be relatively insensitive to the dispersion constant C_o in the range $0.5 < C_o < 2.0$. The effect of the parameter α was also examined, since it has been previously shown, Bini and Jones (2007) that a value of $\alpha = 0.8$ reproduces the observed heavy tails of the particle acceleration distribution. The simulations presented show that droplet accumulation in the different locations of the mixing layer examined is only slightly modified for variations in α in the range 0.5–0.8. Results are reported in terms of the probability density function for droplet diameter at selected downstream locations of the mixing layer. The effects of the droplet inertia were presented in terms of the Stokes number, illustrating that droplets with small diameters ($d < 10\ \mu m$), tend to respond faster to the fluctuations of the gas phase and migrate towards in the unladen zone of the mixing layer. The simulations presented in this work are of scientific interest in the analysis of spray combustion dynamics, since it focuses on the dispersion effects in the near-field of the mixing layer, which is the important region in many combustion processes related particularly to ignition and flame stabilisation.

Acknowledgements

This work received funding from the European Community through the project TIMECOP-AE (Project No. AST5-CT-2006-030828). It reflects only the authors' views and the Community is not liable for any use that may be made of the information contained therein.

References

Bini, M., Jones, W.P., 2007. Particle acceleration in turbulent flows: a class of nonlinear stochastic models for intermittency. Phys. Fluids 19, 035104.
Bini, M., Jones, W.P., 2008. Large Eddy simulation of particle laden turbulent flows. J. Fluid Mech. 614, 207–252.
Brown, G., Roshko, A., 1974. On density effects and large structure in turbulent mixing layers. J. Fluid Mech. 64, 775–816.
Chein, R., Chung, J.N., 1987. Effects of vortex pairing on particle dispersion in turbulent shear flows. Int. J. Multiphas. Flow 6, 785–802.
Chung, J.N., Troutt, T.R., 1988. Simulations of particle dispersion in an axisymmetric jet. J. Fluid Mech. 186, 199–222.
di Mare, L., Klein, M., Jones, W.P., Janicka, J., 2006. Synthetic turbulence inflow conditions for large Eddy simulation. Phys. Fluids 18, 025107.
Elghobashi, S., 1994. On predicting particle-laden turbulent flows. Appl. Sci. Res. 52, 1309329.
Elghobashi, S.E., Truesdell, G.C., 1993. On the two-way interaction between homogeneous turbulence and dispersed solid particles. I: Turbulence modification. Phys. Fluids A 3, 1790–1801.
Gardiner, C.W., 2002. Handbook of Stochastic Methods for Physics. Chemistry and the Natural Science. Springer.
Germano, M., 1992. Turbulence: the filtering approach. J. Fluid Mech. 238, 325–336.
Germano, M., Piomelli, U., Moin, P., Cabot, W.H., 1991. A dynamic subgrid-scale Eddy viscosity model. Phys. Fluids A 3, 1760–1765.
Jimenez, J., Linan, A., Rogers, M.M., Higuera, F.J., 1997. A priori testing of subgrid models for chemically reacting non-premixed turbulent shear flows. J. Fluid Mech. 349, 149–171.
Jones, W.P., Sheen, D., 1999. A probability density function method for modelling liquid fuel sprays. Flow Turbul. Combust. 63, 379–394.
Jones, W.P., di Mare, F., Marquis, A.J., 2002. LES-BOFFIN: Users Guide. Tech. rep., Imperial College London.
Kiger, K.T., Lasheras, J.C., 1997. Dissipation due to particle/turbulence interaction in a two-phase, turbulent, shear layer. Phys. Fluids 9, 3005–3023.
Kulick, J.D., Fessler, J.R., Eaton, J.K., 1994. Particle response and turbulence modification in fully developed channel flow. J. Fluid Mech. 277, 109–134.
Lazaro, B.J., Lasheras, J.C., 1992. Particle dispersion in the developing free shear layer. Part 1: Unforced flow. J. Fluid Mech. 235, 135–178.
Lefebvre, A.H., 1989. Atomization and Sprays. Hemisphere Publishing Corp.
Longmire, E.K., Eaton, J.K., 1992. Structure of a particle-laden round jet. J. Fluid Mech. 236, 217–257.
Lopéz-Pagés, E., Dopazo, C., Fueyo, N., 2004. Very-near-field dynamics in the injection of two-dimensional gas jets and thin liquid sheets between two parallel high-speed gas streams. J. Fluid Mech. 515, 1–31.
Lundgren, T.S., 1967. Distribution functions in the statistical theory of turbulence. Phys. Fluids 177, 969–975.
Martin, J.E., Meiburg, E., 1994. The accumulation and dispersion of heavy particles in forced two-dimensional mixing layers. I. The fundamental and subharmonic case. Phys. Fluids 6, 1116–1132.
Miller, R.S., Bellan, J., 2000. Direct numerical simulation and sub-grid analysis of transitional droplet laden mixing layer. Phys. Fluids 12 (3), 650–671.
Piomelli, U., 1999. Large-Eddy simulation: achievements and challenges. Prog. Aerosp. Sci. 35, 335–362.
Piomelli, U., Liu, J., 1995. Large Eddy simulation of rotating channel flows using a localized dynamic model. Phys. Fluids 7 (4), 839–848.
Smagorinsky, J., 1963. General circulation experiments with the primitive equations. I. The basic experiment. Mon. Weather Rev. 91, 99–164.
Squires, K.D., Eaton, J.K., 1990. Particle response and turbulence modification in isotropic turbulence. Phys. Fluids A 2, 1191–1203.
Squires, K.D., Eaton, J.K., 1991a. Measurements of particle dispersion obtained from direct numerical simulations of isotropic turbulence. J. Fluid Mech. 226, 135.
Squires, K.D., Eaton, J.K., 1991b. Preferential concentration of particles by turbulence. Phys. Fluids A 3, 1169–1178.
Squires, K.D., Eaton, J.K., 1994. Effect of the selective modulation of turbulence on two-equation models for particle-laden turbulent flows. J. Fluids Eng. 116, 778–784.
Tageldin, M.S., Cetegen, B.M., 1997. Development of mixing and dispersion in an isothermal, droplet-laden, confined turbulent mixing layer. Combust. Sci. Technol. 30, 131–169.
Uijttewaal, W., Oliemans, R., 1996. Particle dispersion and deposition in direct and large Eddy simulations of vertical pipe flows. Phys. Fluids 8, 2590–2604.
Vreman, B., Geurts, B., Kuerten, H., 1997. Large-Eddy simulation of the turbulent mixing layer. J. Fluid Mech. 339, 357–390.
Wang, Q., Squires, K., 1996. Large Eddy simulations of particle laden turbulent channel flow. Phys. Fluids 8, 1207–1223.
Wang, Q., Squires, K., 1998. Transport of heavy particles in a three-dimensional mixing layer. J. Fluids Eng. 120, 613–620.
Yeh, F., Lei, U., 1991a. On the motion of small particles in an homogeneous isotropic turbulent flow. Phys. Fluids A 3, 2571–2586.
Yeh, F., Lei, U., 1991b. On the motion of small particles in an homogeneous turbulent shear flow. Phys. Fluids A 3, 2758–2776.
Yuen, M.C., Chen, L.W., 1976. On drag of evaporating liquid droplets. Combust. Sci. Technol. 14, 147–154.